



ELSEVIER

Available online at [www.sciencedirect.com](http://www.sciencedirect.com)

SCIENCE @ DIRECT®

Nuclear Instruments and Methods in Physics Research B 207 (2003) 36–44

**NIM B**  
Beam Interactions  
with Materials & Atoms

[www.elsevier.com/locate/nimb](http://www.elsevier.com/locate/nimb)

## Microstructure and magnetic properties of Co nanoparticles in ion-implanted $\text{Al}_2\text{O}_3$

A. Meldrum<sup>a,\*</sup>, L.A. Boatner<sup>b</sup>, K. Sorge<sup>b</sup>

<sup>a</sup> *Department of Physics, University of Alberta, Edmonton, Canada AB T6G 2J1*

<sup>b</sup> *Solid State Division, Oak Ridge National Laboratory, Oak Ridge, TN 37831, USA*

### Abstract

Ion implantation and thermal processing can be used to create a variety of single-element or compound ferromagnetic nanocrystals embedded in dielectric host materials. This approach leads to the formation of nanocomposites with several attractive characteristics for potential applications in magnetic data storage media. A number of problems must be addressed before such applications can be realized in practice, however. One difficulty lies in the exercise of sufficiently fine control over the magnetic and microstructural properties of interest. Here, we show that Co nanocrystals produced by the ion implantation of  $\text{Al}_2\text{O}_3$  can be formed either as spheroidal or well faceted single-crystal precipitates, depending on the synthesis conditions. Subsequent ion irradiation of the nanoparticles can alter the microstructure and internal chemistry of the particles as well as that of the host matrix, thereby providing a means of increasing the coercive field of the Co nanoparticles by almost two orders of magnitude.

© 2003 Elsevier Science B.V. All rights reserved.

PACS: 81.07.B; 75.50.T; 61.46

Keywords: Nanocrystals; Microstructure; Ion implantation; Co;  $\text{Al}_2\text{O}_3$ ; Magnetic

### 1. Introduction

In recent years, ion implantation has been used to create ferromagnetic nanoscale composites consisting of Fe, Ni or Co precipitates embedded in the near-surface region of a dielectric host such as  $\text{SiO}_2$  or  $\text{Al}_2\text{O}_3$  [1–5]. These composites generally have a low magnetic coercivity and in some cases, they are superparamagnetic at room temperature. Blocking temperatures have been measured and these agree reasonably well with the calculated

values based on the average size of the precipitates. The magnetic moment per ion is similar to that observed in the bulk material and the saturation field is usually less than 5 kG – depending on the implant dose and annealing conditions employed.

In fused  $\text{SiO}_2$ , ion implantation followed by thermal processing produces nanoparticles that are usually spherical in shape and that are normally randomly oriented within the host. As a result, magnetocrystalline anisotropy effects, if observable, are averaged over all directions and cannot be measured on a macroscopic scale. If, however, a crystalline material is used as the host phase, then the resulting nanoparticles are generally aligned crystallographically with the host and, accordingly,

\* Corresponding author. Tel.: +1-780-492-5342; fax: +1-780-492-0714.

E-mail address: [ameldrum@ualberta.ca](mailto:ameldrum@ualberta.ca) (A. Meldrum).

with each other. Depending on the surface energy of the particles and the host, the nanocrystals may also show well-developed crystal facets [6]. An excellent example of this type of faceting was recently documented for Fe-implanted yttrium-stabilized zirconia (YSZ), in which the Fe nanoparticles formed near-perfect “nanocubes” aligned in specific orientations with respect to the cubic axes of the host YSZ [7].

Sapphire is a crystalline material that is frequently used as the host phase in ion implantation/nanocomposite experiments. In previous work, single-crystal sapphire has been implanted with either Co [2] or Fe [5] to produce a composite of crystallographically aligned ferromagnetic nanocrystals. Iron has a body-centered cubic structure at room temperature; whereas for Co, the stable phase at room-temperature has a hexagonal close packed structure. In the case of Co nanocrystals, the situation is more complicated because there is also a face-centered cubic phase (normally stable above 450 °C in the bulk) that can be stabilized at small particle sizes [8]. Previous reports suggest that nanocrystalline Co can, in fact, be a mixture of cubic and hexagonal phases [8,9]. In the case of ion-implanted Al<sub>2</sub>O<sub>3</sub>, the hexagonal structure of the sapphire might be expected to favor the formation of hexagonal Co due to the possible lattice registry between the two phases.

The presence of two crystal structures can complicate the interpretation of the magnetic results, since the magnetocrystalline anisotropy for the two structures is quite different. In previous work, we found that the magnetic coercivity of an Al<sub>2</sub>O<sub>3</sub>–Co composite was ~150 Oe with the magnetic field applied either parallel or perpendicular to the (0001)-oriented sapphire crystal surface normal [2]. The Co nanoparticles in that case were poorly faceted and exhibited a spheroidal shape, as determined from cross-sectional and plan-view TEM images. X-ray diffraction showed that the Co precipitates were predominantly hexagonal, but that there was a minor amount of the cubic Co phase present as well. Co nanoparticles with the hexagonal structure were aligned with their *c*-axis parallel to the *c*-axis of the host sapphire; whereas the cubic nanocrystals were aligned with a [111] axis parallel to the sapphire *c*-axis. Routine  $\theta$ – $2\theta$

scans cannot readily distinguish between the [002] and [111] directions of the hexagonal and cubic cobalt nanoparticles, respectively. Therefore, in previous work, scans were made (i.e. L-scans) along alternative crystallographic directions that can be used to distinguish between the two structures [2].

In investigations carried out subsequent to those reported in [2], but in which the processing conditions were apparently the same [10], we have found that the resulting Co-particles were not rounded but instead were well faceted with excellent growth faces. Accordingly, in the present work we show that, in fact, the microstructure of Al<sub>2</sub>O<sub>3</sub>–Co composites is highly sensitive to the implantation conditions and we examine the role of specimen processing in the development and formation of the various Co-particle/Al<sub>2</sub>O<sub>3</sub>-host microstructures. Additionally, we have extended the previous investigations originally reported in [2] that established that microstructural modifications through ion beam damage can be employed to control and tailor the magnetic properties of Al<sub>2</sub>O<sub>3</sub>–Co composites over a wide range of magnetic behavior.

## 2. Experimental

Two single-crystal *c*-axis-oriented sapphire wafers were implanted with 140 keV Co<sup>+</sup> to a dose of  $8 \times 10^{16}$  ions/cm<sup>2</sup>. In one case (hereafter referred to as specimen “A”), the sample was implanted at room-temperature without heat sinking; while in the other case, the implantation was carried out with the specimen heat sunk to the sample holder and cooled to –100 °C (specimen “B”). After implantation, both specimens were annealed for two hours at 1100 °C under flowing Ar+4% H<sub>2</sub>. Cross-sectional and plan-view transmission electron microscopy and X-ray diffraction were then used to determine the microstructure and orientation of the resulting Co nanoparticles. Preliminary results on specimen A were reported in [2].

In order to illustrate the nature and degree of control over the magnetic properties of Co nanoparticles induced by displacive radiation effects, a Co-sapphire nanocomposite was subsequently irradiated with either 244 keV Xe<sup>+</sup>, 320 keV Pt<sup>2+</sup> or 310 keV Pb<sup>2+</sup> to varying ion fluences. The Xe- and

Pt-implantations were carried out at room-temperature and the Pb implantation was performed at +100 °C. The corresponding dose was calculated by using the Monte Carlo computer code SRIM-2000 [11] in the full cascade mode in order to obtain the number of displacements per ion per nm (using displacement energies for Al and O of 20 and 50 eV, respectively). Since the ion dose varies as a function of depth, for simplicity we will refer to the dose at a depth of 60 nm (corresponding to the approximate center of the Co nanoparticle profile). The microstructure of the resulting composite was characterized by TEM and the magnetic hysteresis was measured either with a SQUID magnetometer or magneto-optically by magnetic circular dichroism.

### 3. Results and discussion

#### 3.1. Formation and microstructure of $Al_2O_3$ -Co nanocomposites

Fig. 1(a) shows a plan-view image of the specimen that was implanted at room-temperature

(specimen A) and subsequently annealed for 2 h at 1100 °C. The particles are spheroidal in shape, although a few of the precipitates show a weak hexagonal faceting. The inset to Fig. 1(a) is an electron-diffraction pattern from this specimen, showing numerous double-diffraction maxima. The double-diffraction spots are consistent with hexagonal Co aligned with its  $c$ -axis parallel to the  $c$ -axis of the host sapphire. The cubic phase could not be unambiguously identified in the diffraction pattern, although in our previous work, X-ray diffraction from this specimen did show the presence of a minor amount of cubic cobalt [2].

Fig. 1(b) shows a plan-view TEM image of the specimen implanted at  $-100$  °C (specimen B) after annealing under identical conditions as for specimen A. In this case, the nanoparticles are well faceted, with good crystal faces parallel to the hexagonal axes of the sapphire. Unlike the case for specimen A, the electron diffraction pattern shows a set of double-diffraction maxima at positions that are intermediate between the brighter maxima from the crystalline sapphire. These new double-diffraction spots, not present in the inset to Fig. 1(a), can be attributed to the cubic  $\gamma$ -phase of

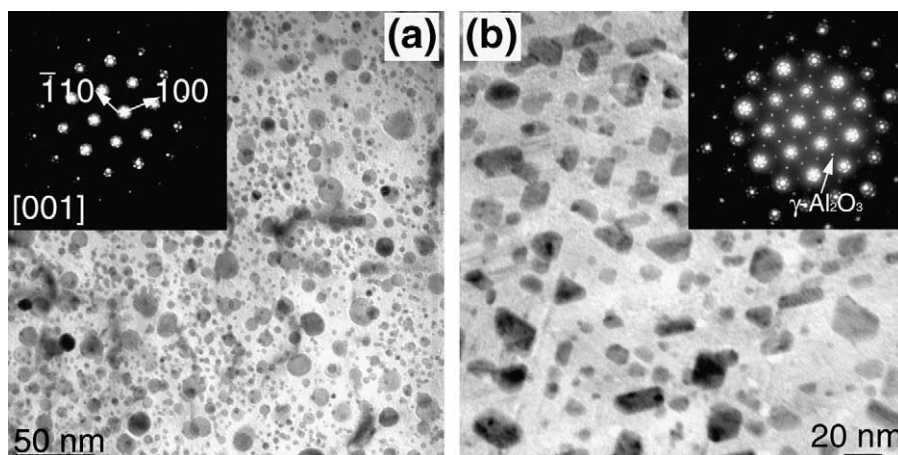


Fig. 1. Plan-view bright-field images and associated electron-diffraction patterns for specimens A and B (see text). The double-diffraction spots for specimen A can be attributed to hexagonal Co aligned with its  $[001]$  axis parallel to the sapphire  $[001]$  (out-of-plane) and a  $[100]$  axis parallel to the sapphire  $[110]$  (in-plane). The rings of faint spots around the bright sapphire maxima are due to top-bottom effects (i.e. diffracted beams passing first through the sapphire and then the Co, or vice versa). In (b), a set of diffraction spots is visible at half-intervals between the main  $(100)$  maxima from hexagonal  $Al_2O_3$ . These are due to  $[111]$ -oriented  $\gamma$ - $Al_2O_3$ . The additional double-diffraction spots (arrow) are due to cubic Co aligned with its  $[111]$  axis parallel to the  $[001]$  axis of the sapphire (out-of-plane) and an  $[422]$  axis parallel to the sapphire  $[100]$  (in-plane).

$\text{Al}_2\text{O}_3$  aligned with its [1 1 1] axis parallel to the  $c$ -axis of the hexagonal  $\alpha$ - $\text{Al}_2\text{O}_3$ . Unlike the case for specimen A, *two* sets of double-diffraction maxima were observed that correspond to the [1 1 1] axis of cubic Co and the [0 0 2] axis of hexagonal Co, respectively.

These results show that the microstructure of the Co-implanted sapphire specimens is highly sensitive to the implantation temperature and these observations explain some of the apparently inconsistent results in the previous work [2,10]. In order to further examine the origin of the faceted particle microstructure, cross-sectional TEM specimens were prepared from specimen B, prior to and after the thermal processing procedure (Fig. 2). After implantation, the host sapphire was amorphized to a depth of 140 nm and there was no evidence for Co nanocrystals in the bright-field images or electron-diffraction patterns. Between 140 and 200 nm, the sapphire is crystalline but highly defective and below  $\sim 200$  nm, there is no implantation damage.

After 2 h at 1100 °C in flowing Ar+4%  $\text{H}_2$ , the microstructure is considerably altered. The sapphire is completely recrystallized and Co nanoclusters precipitated in a layer extending from the surface to a depth of 180 nm. The microstructure of the Co nanoparticles is depth dependent. Below 88 nm, the particles are rounded and appear sim-

ilar in morphology to the particles in specimen A; whereas, at shallower depths the nanoparticles are faceted and appear to be “flattened” parallel to the specimen surface. The cubic and hexagonal phases of  $\text{Al}_2\text{O}_3$  can also be distinguished by electron-diffraction in the cross-sectional images. Between the specimen surface and the boundary at a depth of 88 nm, there is a layer of cubic  $\gamma$ - $\text{Al}_2\text{O}_3$ ; whereas below 88 nm, the  $\text{Al}_2\text{O}_3$  is hexagonal. This specimen, therefore, contains four separate phases: i.e. the hexagonal and cubic forms of both  $\text{Al}_2\text{O}_3$  and Co.

In comparison, the specimen implanted at room-temperature (specimen A) did not become amorphous after the ion implantation (Fig. 3). A defect-rich layer is evident in the cross-sectional image, but there was no indication of amorphization in the electron-diffraction patterns (inset to Fig. 3). After thermal processing, there was no evidence for the formation of  $\gamma$ - $\text{Al}_2\text{O}_3$ ; all the particles were rounded and poorly faceted; and there was no microstructural boundary at a depth of 88 nm – as was the case for specimen B. The cross-sectional TEM results for the annealed specimen were reported in [2].

X-ray diffraction scans in the  $\theta$ - $2\theta$  geometry are shown in Fig. 4 for the two specimens A and B. Peaks corresponding to the [1 1 1] planes of  $\gamma$ - $\text{Al}_2\text{O}_3$  are evident from specimen B, but they are

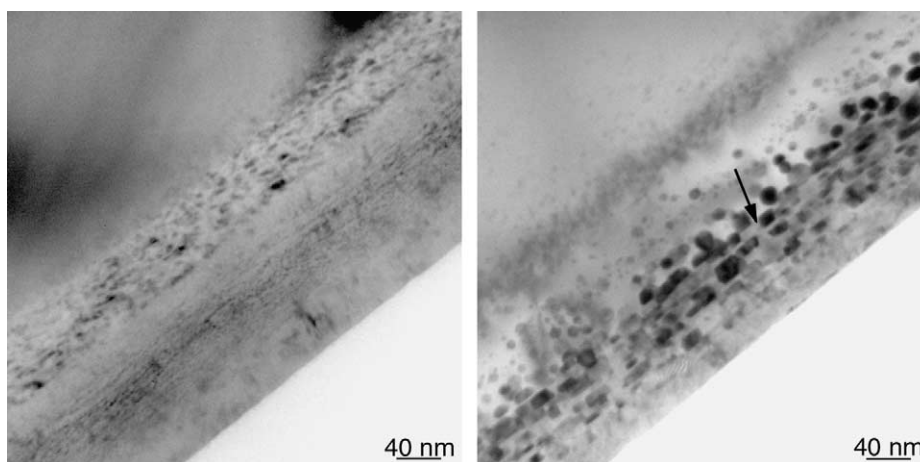


Fig. 2. Cross-sectional TEM micrographs for specimen B; (left): as implanted and (right) after thermal processing for 2 h at 1100 °C in Ar+4%  $\text{H}_2$ . The arrow marks the boundary between the faceted particles nearer to the surface and the rounded ones at greater depths.

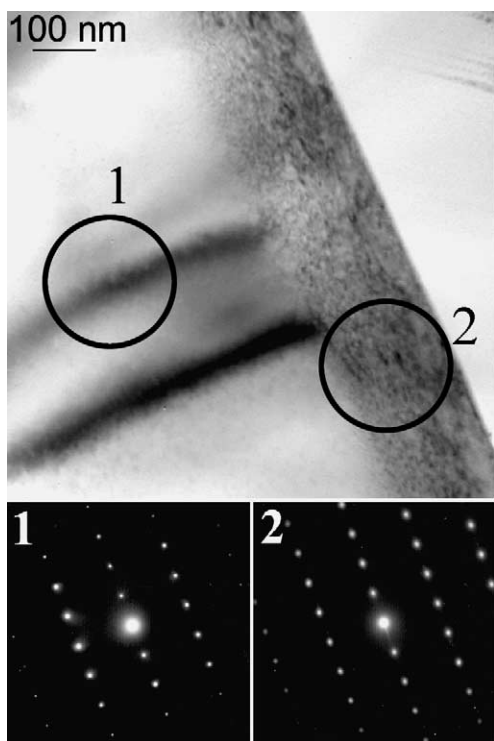


Fig. 3. Cross-sectional TEM micrograph of an  $\text{Al}_2\text{O}_3$  specimen implanted with Co at room-temperature. The sapphire did not become amorphous.

absent from specimen A, in agreement with the TEM results. We did not have access to a 4-circle diffractometer for this study and were, therefore, limited to surface normal scans in which it is very difficult to distinguish between cubic and hexagonal Co. For both samples, the Co peak was relatively wide, suggesting a possible mixture of the hexagonal and cubic cobalt (the  $[111]_{\text{cubic}}$  and  $[002]_{\text{hexagonal}}$  spacings have a difference of  $0.5^\circ$  in  $2\theta$ ). Electron-diffraction results suggest that more cubic Co may be present in specimen B, but the results cannot be quantified and are, therefore, not conclusive.

The complex microstructure of this specimen is due to a variety of processes that occur in the host sapphire during the implantation and subsequent annealing. If the sapphire becomes amorphous during implantation, it can recrystallize epitaxially during the thermal processing stage. Cubic  $\gamma\text{-Al}_2\text{O}_3$  is a metastable phase that forms during the

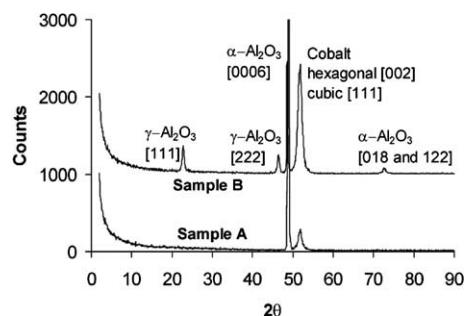


Fig. 4. X-ray diffraction scans in the  $\theta$ - $2\theta$  geometry. The results for sample B are offset for clarity.

recrystallization of ion-beam-amorphized sapphire [12]. According to [13], the cubic phase “slowly” transforms to stable  $\alpha\text{-Al}_2\text{O}_3$  at  $\sim 1000^\circ\text{C}$ . In the present case, annealing at  $1100^\circ\text{C}$  did not complete the cubic-to-hexagonal transformation. The greater abundance of cubic Co nanocrystals in specimen B (according to electron-diffraction) is probably due to the fact that the particles initially grew within the layer of cubic  $\text{Al}_2\text{O}_3$ , whereas hexagonal Co is preferred if it forms in hexagonal  $\text{Al}_2\text{O}_3$ . This type of crystallographic registry was previously reported for Ge and CdSe nanocrystals formed by the ion implantation of  $\text{Al}_2\text{O}_3$  [14].

Both specimens A and B are soft magnets at room-temperature, with relatively low coercivity with the magnetic field applied perpendicular to the plane of particles. More detailed magnetic measurements are currently ongoing to determine the magnetic effects of the precipitate microstructure observed by TEM. Measurements parallel to the in-plane crystallographic directions of the sapphire are expected to show differences due to the magnetocrystalline anisotropy of hexagonal versus cubic particles. The relative crystalline perfection of the faceted particles may also play a significant role, since the magnetic properties of nanocrystalline materials can be strongly dependent on the nature of the nanoparticle-host interface [15].

### 3.2. Irradiation-induced microstructural and magnetic modifications

Modifying the microstructure of the Co nanoparticle/host  $\text{Al}_2\text{O}_3$  system *subsequent* to

nanoparticle formation can also have profound effects on the magnetic properties. In previous work, we demonstrated that irradiation of a type A specimen with either 244 keV Xe or 320 keV Pt ions at ambient temperature can dramatically modify the magnetic coercivity [2]. In the case of the Xe implantation, the coercivity (magnetic field applied parallel to the surface normal) increased from 150 G to  $\sim 500$  G, while the Pt-implanted specimen achieved the highest coercivity (1.14 kG). For both Xe- and Pt-irradiated samples, the coercivity increases rapidly at first, but then reaches a saturation value at an irradiation dose of approximately 20 dpa (Fig. 5). In contrast, when the magnetic field was applied parallel to the specimen surface, the coercivity was virtually unchanged after irradiation (Fig. 6).

Finally, in separate work, we also irradiated an  $\text{Al}_2\text{O}_3$ -cubic Co nanoparticle composite (initially implanted with 140 kV Co to a fluence of  $5 \times 10^{16}$  ion/cm<sup>2</sup> and annealed for 1 h at 1000 °C in ArH<sub>2</sub>) with 320 keV Pb ions at a temperature of +100 °C. Pb was selected in order to maximize the displacive radiation damage at a given temperature. In this case, however, the coercivity of the specimen remained virtually unchanged up to doses in excess of 20 dpa, thereby suggesting the possible presence of cubic particles.

Transmission electron microscopy studies were carried out in order to investigate the micro-

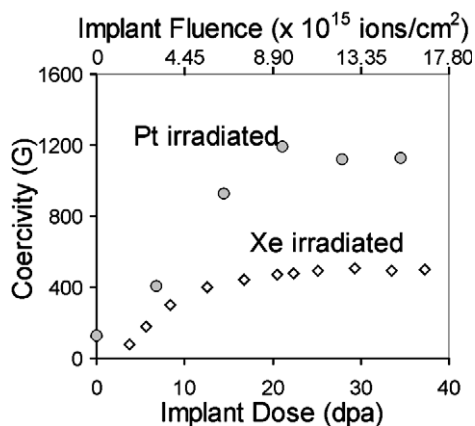


Fig. 5. Variation of the coercive field as a function of dose for Xe- and Pt-implantation of specimen A. The field was applied parallel to the specimen normal (after [2]).

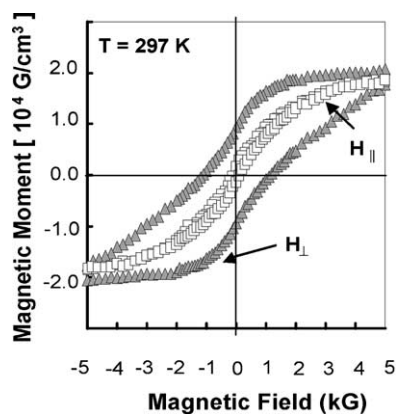


Fig. 6. Magnetic hysteresis measurements for the  $\text{Al}_2\text{O}_3$ -Co nanocomposite implanted with  $6.4 \times 10^{15}$  ions/cm<sup>2</sup> of Pt. Measurements are shown for the magnetic field applied parallel and perpendicular to the plane of Co precipitates (after [2]).

structural characteristics responsible for the observed magnetic effects. Fig. 7 shows plan-view and cross-sectional TEM micrographs of an  $\text{Al}_2\text{O}_3$ -Co nanocomposite (specimen A) implanted with Xe to a fluence of  $9 \times 10^{15}$  ions/cm<sup>2</sup>. In plan-view, the particles are well rounded and any trace of faceting has disappeared. A few of the particles display a mottled internal contrast, possibly due to the incorporation of Xe at vacancy clusters (a process well known in the gas-ion implantation of silicon [e.g. see [6]]). An electron-diffraction pattern is shown in the inset, with the double-diffraction maxima consistent with hexagonal Co. In cross-section, it is apparent that the sapphire has, in fact, been amorphized from the surface to a depth of 120 nm and that most of the Co nanoclusters are embedded within this ion-beam-amorphized layer. The particles are rounded, have internal contrast features consistent with the presence of vacancy clusters or gas bubbles, but they do not show any evidence of amorphization. This represents a rather unusual microstructure in which crystallographically aligned nanoparticles are embedded in an amorphous matrix – similar to the case of ZnS nanocrystals reported in [16].

Fig. 8 shows the TEM results for the Pt-implanted specimen. Similar to the case for the Xe implantations, all trace of precipitate faceting is

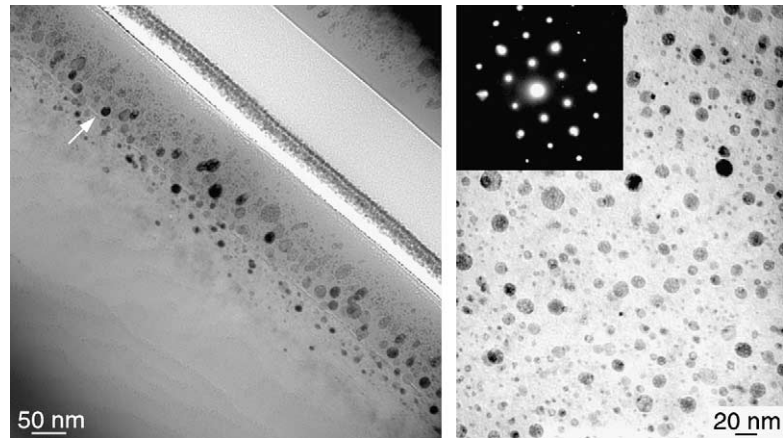


Fig. 7. Cross-sectional (left) and plan-view (right) images of specimen A after implantation of Xe to a fluence of  $9 \times 10^{15}$  ions/cm<sup>2</sup>. The images were tilted away from a zone axis to minimize the diffraction contrast due to damage and strain. The Al<sub>2</sub>O<sub>3</sub> was amorphized to a depth of 140 nm. The arrow in the cross-sectional image marks the position of the crystalline–amorphous boundary.

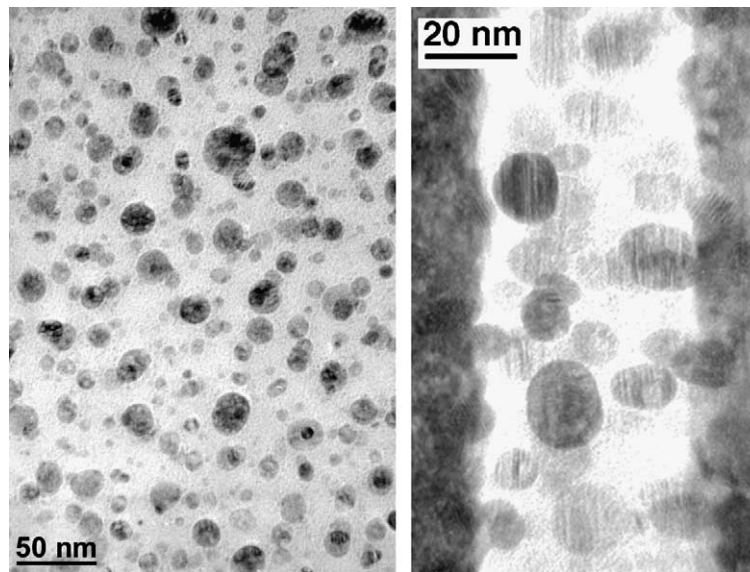


Fig. 8. Cross-sectional and plan-view images of specimen A after implantation of Pt to a fluence of  $6.4 \times 10^{15}$  ions/cm<sup>2</sup>.

lost; many of the particles contain a mottled internal contrast and the nanoparticles are still crystalline. Once again, the sapphire has been amorphized, but in this case, the amorphous layer is buried below the surface. Most of the Co nanoclusters are embedded within the buried amorphous layer. Chemical maps for this specimen are shown in Fig. 9. The Co nanoclusters are clearly

visible against the background Al<sub>2</sub>O<sub>3</sub>. The Pt appears to follow a roughly Gaussian implantation profile and it is not preferentially located within the particles. This suggests that alloying between Co and Pt (to form an extremely hard magnetic alloy of CoPt) does not occur to a significant degree. Of course, some small fraction of the implanted Pt is located within Co nanoparticles and

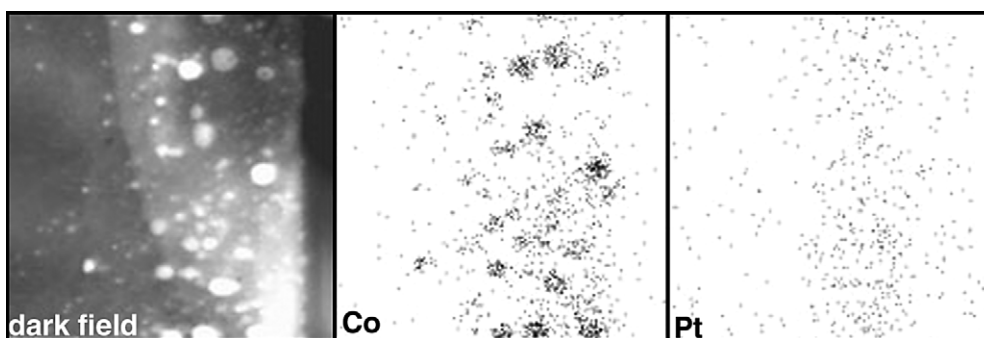


Fig. 9. Dark-field image and corresponding energy-dispersive X-ray maps for the Pt-implanted ( $6.4 \times 10^{15}$  ions/cm<sup>2</sup>) Al<sub>2</sub>O<sub>3</sub>-Co nanocomposite.

it is possible that dilute atomic-scale domains of CoPt may exist.

Microstructurally, the Xe- and Pt-implanted nanocomposites are similar. In the case of the Pb implantation, the Co nanoclusters had a similar appearance as in the above two cases but, in contrast, the sapphire was not amorphized because the implantation was carried out at +100 °C. The results can, therefore, be summarized as follows:

1. Ion irradiation can dramatically increase the magnetic coercivity of hexagonal Co nanoparticles parallel to the host surface normal, but not perpendicular to it.
2. Room-temperature irradiation of hexagonal Co particles with Xe or Pt causes a complete loss of precipitate faceting and amorphizes the host sapphire.
3. Irradiation at +100 °C with Pb has a similar effect on the microstructure of the Co nanoparticles, but the sapphire is not amorphized.
4. When the Pb irradiation is done at +100 °C, there is no dramatic jump in the Co-particle coercivity in either direction of the applied field.

In this case, however, a cubic Co phase may have been formed by annealing at 1000 °C rather than annealing at 1100 °C as in the case of samples A and B.

In hexagonal Co, the *c*-axis is the magnetic easy axis and the coercivity is, therefore, highest for a magnetic field applied parallel to this direction. When sapphire is ion-beam-amorphized, it experiences significant strain and volume expansion.

The compressive strain associated with this volume expansion is partially relieved by swelling parallel to the surface normal [17]. Differential stresses during the swelling of the host Al<sub>2</sub>O<sub>3</sub> can alter the anisotropy energy due to magnetoelastic effects. This can, in principle, modify the anisotropy energies and this effect might, in part, account for the large effect observed upon ion irradiation of the Co nanoparticle/Al<sub>2</sub>O<sub>3</sub>-host nanocomposite. Three of the four magnetostriction coefficients for cobalt at room-temperature are negative, but there appears to be some disagreement as to the actual values [18].

A number of experiments remain to be done to clarify the mechanism or mechanisms associated with the observed relatively large heavy-particle irradiation-induced increase in the coercivity of Co nanoparticles formed in single-crystal Al<sub>2</sub>O<sub>3</sub>. If the structural modifications in the sapphire are important, then the magnetic effects should saturate once the sapphire has been fully amorphized. Previous work using RBS analysis concluded that Xe fluences in excess of  $10^{17}$  ions/cm<sup>2</sup> are required to amorphize sapphire at room temperature [19]. However, the current TEM results (as well as an in situ TEM investigation using 200 keV Pb<sup>2+</sup>: Meldrum, unpublished data) show that sapphire with embedded Co nanoclusters becomes electron-diffraction amorphous in the range of  $10^{16}$  ions/cm<sup>2</sup> for heavy ions (mass equivalent to Xe or greater). Thermal annealing of the high-coercivity specimens will decrease the strain associated with the radiation damage and this can lower the coercivity as observed in the case of Pt-implanted Co

nanoparticles in sapphire. Other effects may play a role – e.g. impurities and defects within the Co nanoparticles may act to effectively “pin” the magnetization and increase the coercivity.

#### 4. Conclusions

The properties of ferromagnetic nanocomposites produced by ion implantation are of increasing technical interest. To date, much of the work has been done on relatively simple systems consisting of Fe, Co or Ni implanted into either fused SiO<sub>2</sub> or crystalline  $\alpha$ -Al<sub>2</sub>O<sub>3</sub>. The present results show that the microstructure of Co nanoparticles formed by ion implantation of Al<sub>2</sub>O<sub>3</sub> can be rather complex and can, to a large degree, be controlled by appropriate selection of the ion implantation conditions. The microstructural and magnetic properties of the resulting Al<sub>2</sub>O<sub>3</sub>–Co composites can be dramatically modified by subsequent ion irradiation leading to a large increase in the plane-perpendicular coercivity. TEM results show that the host sapphire can become amorphous during the room-temperature implantation of Xe or Pt, but not after the implantation of Pb at +100 °C. Investigations are currently ongoing to delineate the role played by thermal annealing effects in the Co-particles versus potential particle-host interactions associated with the amorphization (or lack thereof) of the sapphire host. The continuing studies will also investigate the possible role of finer-scale magnetic effects caused by particle faceting and magneto-crystalline anisotropy in Co-implanted Al<sub>2</sub>O<sub>3</sub>.

#### Acknowledgements

Financial support for this work was provided by NSERC [AM] and the USDOE Division of Materials Sciences [LAB and CWW]. Research sponsored by the Laboratory Directed Research & Development Program of Oak Ridge National Laboratory, managed by UT-Battelle, LLC, for

the US Department of Energy under Contract no. DE-AC05-00OR2725. Diane Caird is thanked for the XRD measurements.

#### References

- [1] A. Meldrum, R.F. Haglund, L.A. Boatner, C.W. White, *Adv. Mater.* 13 (2001) 1431.
- [2] S. Honda, F.A. Modine, T.E. Haynes, A. Meldrum, J.D. Budai, K.J. Song, J.R. Thompson, L.A. Boatner, *Mat. Res. Symp. Proc.* 581 (2000) 71.
- [3] E. Cattaruzza, F. Gonella, G. Mattei, P. Mazzoldi, D. Gatteschi, S. Sangregorio, M. Falconieri, G. Salvetti, G. Battaglin, *Appl. Phys. Lett.* 73 (1998) 1176.
- [4] O. Cántora-González, C. Estournès, D. Muller, J. Guille, J.J. Grob, *Nucl. Instr. and Meth. B* 147 (1999) 422.
- [5] E. Alves, C. MacHargue, R.C. Silva, C. Jesus, O. Conde, M.F. da Silva, J.C. Soares, *Surf. Coat. Technol.* 128 (2000) 434.
- [6] A. Meldrum, S. Honda, C.W. White, R.A. Zuhr, L.A. Boatner, *J. Mater. Res.* 16 (2001) 2670.
- [7] S. Honda, F.A. Modine, A. Meldrum, J.D. Budai, T.E. Haynes, L.A. Boatner, *Appl. Phys. Lett.* 77 (2000) 711.
- [8] R.H. Kodama, A.S. Edelstein, *J. Appl. Phys.* 85 (1999) 4316.
- [9] T. Hayashi, S. Hirono, M. Tomita, S. Umemura, *Nature* 381 (1996) 772.
- [10] A. Meldrum, K.S. Beaty, M. Lam, C.W. White, R.A. Zuhr, L.A. Boatner, *Mater. Res. Soc. Symp. Proc.*, 703, in press.
- [11] J.F. Ziegler, SRIM 2000, IBM-Research, Yorktown, NY, 2000.
- [12] C.W. White, C.J. McHargue, P.S. Sklad, L.A. Boatner, C.G. Farlow, *Mater. Sci. Rep.* 4 (41) (1989).
- [13] International Centre for Diffraction Data, Powder Diffraction File Release 2000, Card #10-0425.
- [14] J.D. Budai, C.W. White, S.P. Withrow, M.F. Chisholm, J.G. Zhu, R.A. Zuhr, *Nature* 390 (1997) 384.
- [15] E.g. see F.J. Himpsel, J.E. Ortega, G.J. Mankey, R.F. Willis, *Adv. Phys.* 47 (1998) 511, for a discussion of magnetic surfaces.
- [16] A. Meldrum, R.A. Zuhr, E. Sonder, J.D. Budai, C.W. White, L.A. Boatner, D.O. Henderson, R.C. Ewing, *Appl. Phys. Lett.* 74 (1999) 697.
- [17] R. Brenier, N. Canut, S.M.M. Ramos, P. Thevenard, *Nucl. Instr. and Meth. B* 90 (1994) 339.
- [18] E.P. Wohlfarth, in: E.P. Wohlfarth (Ed.), *Ferromagnetic Materials*, North-Holland, Amsterdam, 1980.
- [19] C.J. McHargue, G.C. Farlow, C.W. White, B.R. Appleton, P. Angelini, H. Naramoto, *Nucl. Instr. and Meth. B* 10–11 (1985) 569.